Materials Research Proceedings 41 (2024) 2595-2606 https://doi.org/10.21741/9781644903131-285

Experimental and numerical investigation of the light scattering of the 3D printed parts

NGUYEN Thi-Ha-Xuyen[1,a], AKUÉ ASSÉKO André Chateau[1,b], LE Anh-Duc[1] and COSSON Benoît[1,c]

[1]IMT Nord Europe, Institut Mines Télécom, University of Lille, Centre for Materials and Processes, Lille, F-59653 Villeneuve d'Ascq, France

[a]thi-ha-xuyen.nguyen@imt-nord-europe.fr, [b]andre.chateau.akue@imt-nord-europe.fr, [c]benoit.cosson@imt-nord-europe.fr

Keywords: Transmission Laser Welding (TLW), 3D-Printed Thermoplastic Parts, Light Scattering, X-Ray Tomography Images, Ray-Tracing Simulation

Abstract. Anisoprint is a forefront technology in the realm of 3D printing and has ushered in a transformative era in composite material fabrication. The synergistic fusion of Anisoprint's 3D printing technology with laser transmission welding has enabled the creation of complex structures featuring carbon fiber reinforcements along all three spatial axes. This innovative amalgamation empowers the production of components distinguished by their unparalleled strength and precision. In the pursuit of this objective, the integration of transparent thermoplastic windows within 3D-printed components has been employed as conduits for laser beams during the welding process. Nevertheless, the interaction between laser beams and these transparent windows introduces a phenomenon characterized by beam diffusion, primarily attributed to the intrinsic porosity inherent in the 3D printing process. Within the scope of this study, an in-depth examination of laser beam diffusion within 3D-printed carbon fiber components is undertaken. This endeavor encompasses the application of micro-tomography to meticulously construct a comprehensive mesh representing the microstructural intricacies of the transparent section. Leveraging this mesh, ray tracing simulations are conducted to elucidate laser beam behavior. Subsequently, a comparative analysis is conducted between these numerical outcomes and experimental observations, involving the scrutiny of laser beam photographs as they traverse the printed component. This research aspires to enhance our comprehension of the intricate dynamics governing laser beam interactions within Anisoprinted structures. Ultimately, this will contribute to the refinement of laser welding processes and foster the advancement of more efficient and dependable manufacturing methodologies for composite materials.

Introduction

Three-dimensional (3D) printing is one of the potential and major manufacturing processes for fabricating 3D advanced composite parts in more flexible ways than those using molds, thus meeting the expectations of the industry of the future [4,19,20]. Using this advanced fabrication additive, various types of materials are used layer by layer according to given digital CAD data to fabricate complex and personal geometry pieces in a bottom-up manner [5]. 3D printing of continuous carbon fiber reinforced composites (CCFRCs) has demonstrated impressive capabilities in delivering superior mechanical properties and creating lightweight structures [13,15]. In the family of 3D-printed technologies, you can find the technology of Material Extrusion (MEX - Fig. 1). However, these processes for continuous fiber composite parts are also limited by the orientation of the fibers remaining in the printing plane, thus allowing high mechanical performance only in this fiber direction. One way to address this technological challenge is to utilize a hybrid approach that combines method 3D printing and Transmission Laser Welding (TLW). The hybrid method aims to create structural parts with high mechanical

properties, which is impossible with 3D printing of thermoplastics, even when filled with short staple fibers.

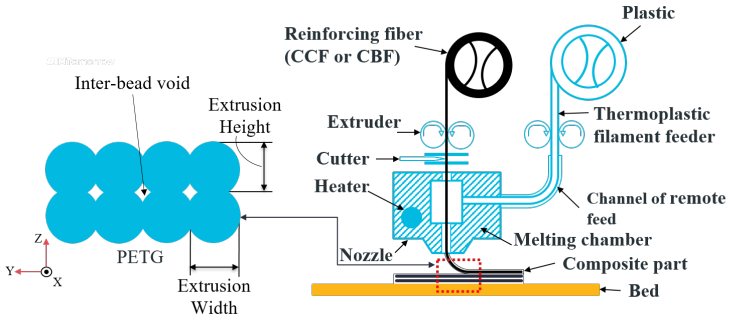

Fig. 1 ANISOPRINT 3D Printing solution for continuous fiber composites

In TLW, two components are used: one is transparent (semi-transparent) at the laser wavelength and the other is an absorbent part at the same wavelength. Before the welding process starts, the components are aligned together. Then, the laser beam energy passes through the transparent (semi-transparent) material and gets absorbed into the interface of both materials (Fig. 2). This heats up the interface of the substrate and triggers the melting and fusion of the materials, resulting in a bond creation between the two parts when the temperature is greater than the melting point in this area. The well-established bonding strength between welded parts depends on both an optimal temperature distribution within the heat-affected zone and a controlled welding time.

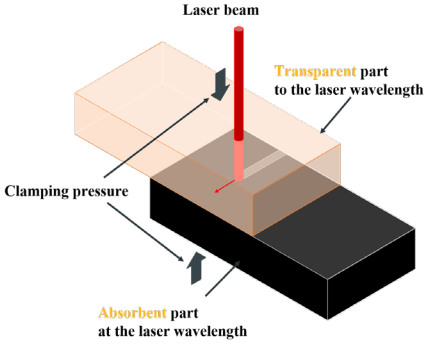

Fig. 2 Transmission Laser Welding (TLW)

Achieving the success of TLW of two components requires careful control of the laser beam profile within the materials and the welding interface. Accurate estimation of the laser beam profile is essential to determine the heat source reaching the interface and to predict the temperature field during the TLW. This temperature is affected by multiple factors, including the optical and thermal properties of the components being welded using the TLW process [2,3,12]. As the laser beam propagates through highly heterogeneous and anisotropic materials, it introduces a new challenge. Due to the 3D-printed component that contains a substantial amount of voids, new phenomena are involved in parallel: uneven transmission and light scattering. This occurrence results in laser beam scattering, which decreases the amount of transmitted energy reaching the weld interface [10]. As a consequence, it directly impacted the quality of welds because of an energy reduction.

It has been demonstrated that the transmissivity and scattering behavior of thermoplastic 3D-printed components are a function of 3D printing process parameters [11]. In this study, we aim to comprehensively investigate the impact of light scattering on the 3D-printed parts. We propose to utilize X-ray micro-tomography to meticulously construct a comprehensive mesh representing the 3D-printed microstructures (Fig. 3) and a ray-tracing model to simulate the optical paths of the laser beam through the 3D-printed part[16,18]. Using this model, it is possible to predict the

changes in the laser heat source distribution at the welded interface, which directly elucidates the impact of the light-scattering effect within the microstructure of the parts.

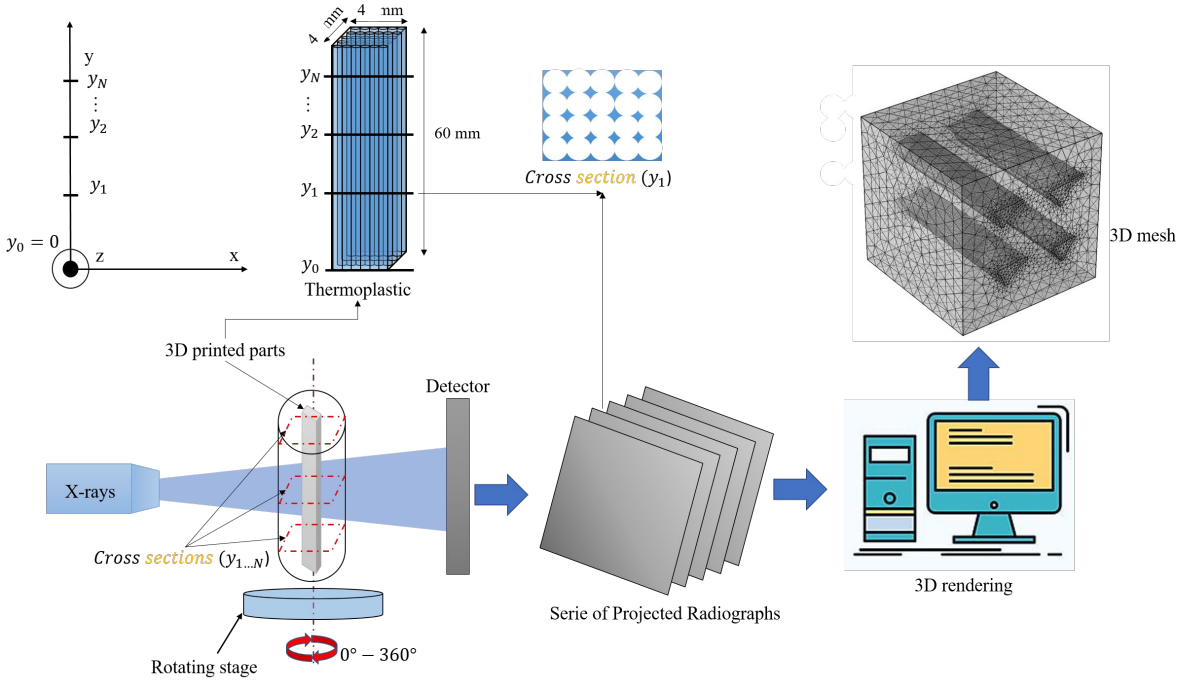

Fig. 3 Schema of the process using the X-ray tomography

Different engineering aspects have been presented with X-ray CT to provide the three-dimensional evaluation of defects inside of the structure in one process [14]. In the actual context, several examples are shown and described utilizing micro CT in the evaluation of 3D-printed components using images of the cross-section of composite materials with micron-sized resolution. Yu et al. [21] performed high-resolution X-ray microscopy and microstructural analysis to study the structure and mechanical properties of 3D-printed fiber-reinforced PLA composites. Chen et al. [6] presented the characterization of air-void systems in 3D-printed cementitious materials using image scanning and X-ray computed tomography. These investigations have researched the influence of the microstructure of the 3D-printed components on the mechanical properties of the materials.

As a first step, the microstructure of the samples printed under different printing parameters will be examined by micro CT. According to the microstructure analysis, the numerical RVEs of the samples will be generated. Subsequently, ray-tracing simulations will be performed to model the diffusion patterns of light scattering through the samples. Then, the transmitted laser beam distributions will be generated at the weld interface and compared for different samples. Finally, a 3D transient thermal model of the TLW process will be conducted using the FEM software COMSOL Multiphysics®. The thermal model will be able to confirm the influence of the scattering effect on the temperature field during the TLW process and the quality of the weld could be predicted.

Experimental section

Materials and processing

The specimens used for the experimental X-ray micro-tomography in this study were produced using an extrusion-based fused filament fabrication process, as illustrated in Fig. 1, which depicts the MEX process. The filaments were composed of Polyethylene terephthalate Glycol (PETG) and carbon fiber-reinforced polymer composites. Polymaker™ supplied the materials in the form of 1.75mm diameter filaments. According to the supplier, the material is characterized by a density

of 1.25g/cm^3 and a glass transition temperature of 81°C. The recommended nozzle temperature ranges from 230°C to 260°C. The 3D CAD models that were employed to manufacture the welding specimens have a rectangular bar shape with dimensions of 60 × 40 × 4mm^3. The nozzle temperature was set to T_n = 240°C, and the bed temperature was set to T_b = 75°C. Except for the parameters listed in Table 1, all other printing parameters were kept constant, with the layer thickness varied between 0.2mm and 0.4mm. For the sample used for tomography, we cut the samples to size 60 × 4 × 4mm^3.

Table 1 MEX processing parameters used in this study

Processing parameters	Values
Nozzle temperature [℃]	240
Nozzle diameter [mm]	0.4
Bed temperature ℃	75
Print speed [mm/s]	30
Layer thickness [mm]	0.2 – 0.4
Infill pattern	Line
Infill percentage [%]	100
Extrusion multiplier	1

Sample microstructures investigation

The microstructural rendering of the droplet-based 3D printing process is evaluated using a 3D imaging technique based on X-ray micro-tomography. Image acquisition is performed using the X ISIS4D (In Situ Innovative Set-ups) equipment, with the following acquisition parameters: a 230 kV X-ray source, a variable detector, that can produce a voxel size ranging from 0.4 to 120 µm. For this study, the voxel size is 5 µm for all scans. The resolution is obtained with the high power source. We obtained 2D images corresponding to each cross-section, as illustrated in Fig. 3.

Table 2 Step by step to construct 3D mesh

1. Preprocessing – Separation of the individual voxelized porosity of each sample using the software GIMP
2. Using a MATLAB algorithm to clearly generate a binary image that separates two zones representing porosity and PETG (Fig. 4)
3. Constructing a 3D mesh using the COMSOL Multiphysics software
3.1 Importing the binary image
3.2 Running a curve to reconstruct the contour of each porosity
3.3 Using the function ‘extrude’ to construct a 3D contour of porosity
3.4 Constructing a cube around all porosity to create a 3D model (Fig. 5). Thanks to this 3D model, it is easy to generate a 3D mesh
4. Exporting the mesh.mphtxt file to import this mesh into the ray-tracing simulation to predict the laser distribution at the interface

To describe the microstructure of the 3D printed part, we used a cross section of the tomography results. Idealized astroid-shaped and half astroid-shaped voids are considered to represent four typical sample types (I, II, and III), each with variable layer thicknesses of e = 0.2mm, e = 0.3mm, and e = 0.4mm, respectively. The form of the voids is computed based on the measured porosity from experimental tomography images as shown in Table 2 (see Fig. 4). The data used in this study are listed in Table 3.

Table 3 Size of the voids

Samples	Layer thickness [mm]	Composition of the sample	Porosity (%)	Volume fraction of the filament PETG (V_f [%])
Type I	0.2	PETG, Air	1.88	98.12
Type II	0.3	PETG, Air	7.01	92.99
Type III	0.4	PETG, Air	5.39	94.61

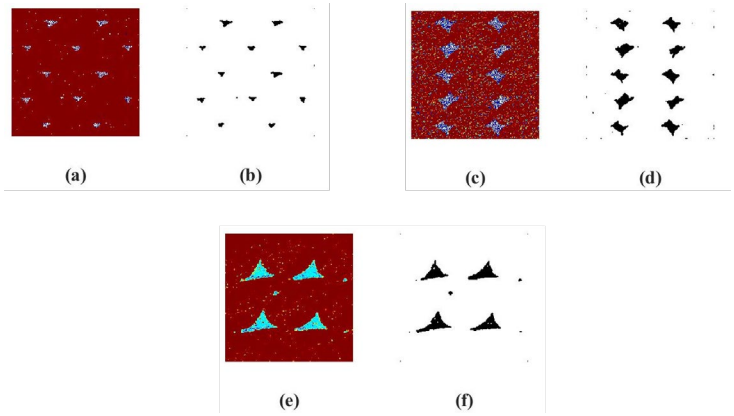

Fig. 4 Void morphology of the 3D printed parts and image analysis procedure to find the void fraction. (a, c, and e) Unprocessed tomography images (b, d, and f) Post-processed images

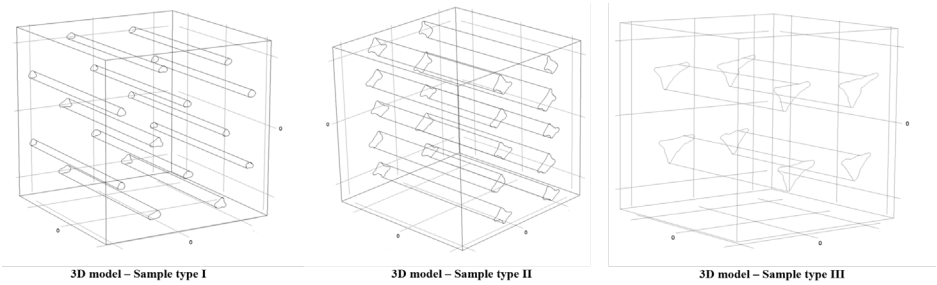

Fig. 5 Generation of the microstructure of the 3D printed parts (I 1x1x1 mm^3; II 1.5x1.5x1.5 mm^3; III 1.2x1.2x1.2 mm^3)

Numerical section

Ray-tracing simulation

According to the description of the interaction between the laser beam and the 3D-printed part, the ray-tracing method is chosen. This method allows us to follow the propagation of the laser beam into a complex structure. In previous studies, the ray-tracing method has been successfully employed to simulate the transmission laser welding (TLW) through the thermoplastic glass fiber composite (polymer + continuous glass fibers) [7,8]. In this method, the laser beam is discretized into a set of rays, and then the path of each ray is followed in the model geometry. Therefore, the ray-tracing method is able to take-into-account the different optical effects of light through the materials, such as refraction, and absorption. In the case of semi-transparent 3D-printed parts, the laser beam diffuses through the complex heterogeneous microstructure due to the numerous refractions occurring at the matrix/void interfaces.

In a complex structure, the propagation of laser beams can be simulated using the ray-tracing method which is based on a Snell-Descartes law [17]:

$$n_1 \sin\theta_1 = n_2 \sin\theta_2 \quad (1)$$

where n_i and θ_i are the refractive indices of the medium i and the angle formed by ray and normal at the interface (see Fig. 6). The refractive indices of the polymer and the voids are respectively n_m = 1.49 and n_v = 1. The reflection of light at the diopter is considered to be negligible in front of refraction [8].

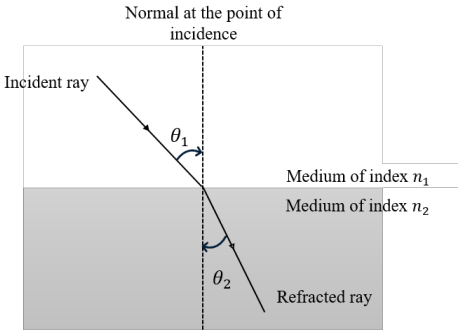

Fig. 6 Transmission of a laser beam through two different media

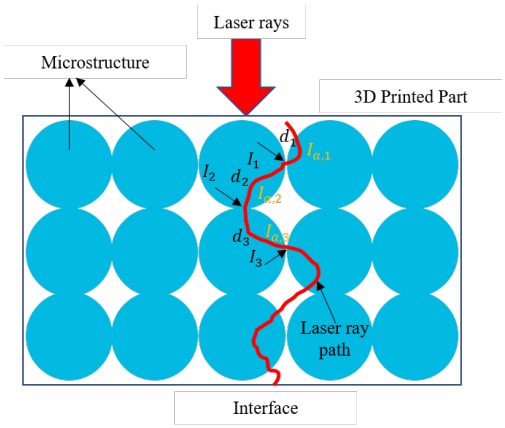

Fig. 7 Path of a ray projection in semi-transparent part

Generally, laser energy absorption is considered only at the weld interface and in the absorbent part. These analytical approaches take into account the Beer-Lambert law to calculate the intensity profile during the laser propagation through the semi-transparent part [22]:

$$I = I_0 e^{-K_h \times d_h} \quad (2)$$

Where I_0 is the initial intensity of the laser beam, K_h is the absorption coefficient (mm^{-1}) of the 3D-printed thermoplastic part, d_A represents the ray path length, and I is the lase the final laser intensity at the weld interface.

The ray-tracing simulations are carried out with a focused beam having a focal angle as seen in the welding machine. Fig. 7 shows an example of the path of a ray that is traveling through the thickness of the semi-transparent part. The distance traveled by each ray in every macro-element is calculated during the ray-tracing simulation. For each macro-element, the Beer-Lambert theory is applied to determine the attenuation of the laser intensity of every ray when it propagates through each macro-element. When Beer-Lambert law is applied to a macro-element n, the intensity of a ray after traveling through the macro-element can be written as:

$$I_n = I_{n-1} \times e^{K_h d_h} \quad (3)$$

The difference in intensity in every macro-element is given by (see Fig. 7):

$$I_{a,n} = I_{n-1} - I_n \quad (4)$$

In this work, the ray-tracing simulations are carried with a focused beam having a focal angle in the welding machine. The beam is discretized into 2400 rays.

Thermal simulation

The temperature field will vary depending on the applied radiative source. This discrepancy arises due to the distinct surface characteristics of intensity distribution between the two cases.

COMSOL Multiphysics® software is a solver for multiphysics simulations using finite elements. This software is used to model heat transfer during transmission laser welding. The heat transfer in the interface of the solid COMSOL is used to model heat transfer in solids by conduction, convection, and radiation. In this study, transmission laser welding is modeled by a radiation source to show the key role of the distribution.

A 3D thermal model of TLW is considered to obtain the temperature field at the interface by solving the energy balance equation [9,12]:

$$\rho C_p \frac{\partial T}{\partial t} = -\nabla \cdot \left(-k\vec{\nabla}T\right) + Q \quad (5)$$

where ρ is the material density, C_p is the specific heat, T is the temperature, t is the time, k is the thermal conductivity, Q is the heat source and ∇ is the gradient operator.

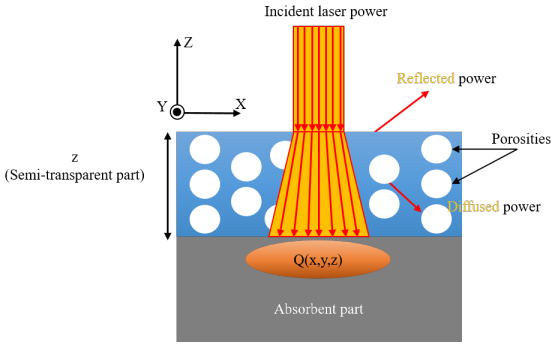

Fig. 8 The heat source of the welded interface during TLW

The laser irradiation is modeled by volume heat source in the absorbent part with the following equation [1] (see Fig. 8):

$$Q(x,y,z) = I(x,y,z) \times K_A \times e^{-K_A \times z} \quad (6)$$

where z is the distance from the interface to the semi-transparent part and K_A is the homogenized absorption coefficient of the 3D printed thermoplastic part. $I(x,y,z)$ is the intensity profile given by the ray-tracing model.

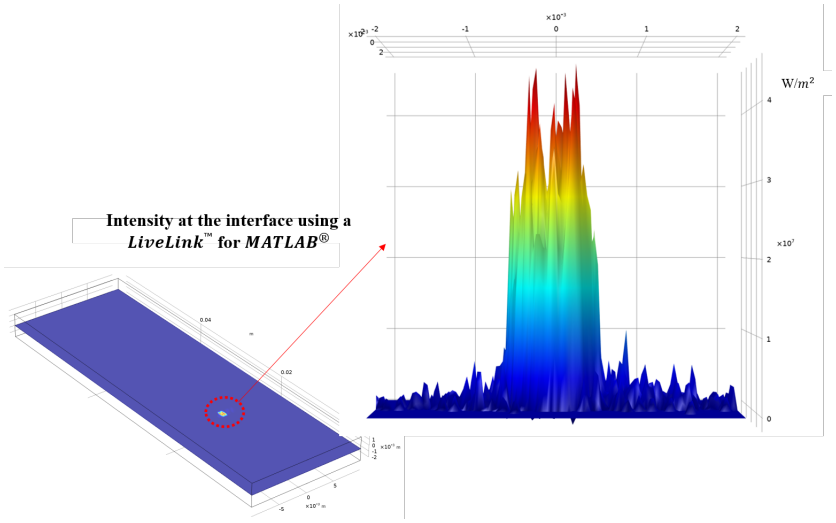

Fig. 9 Numerical model geometry with a surface heat source for thermal simulations

Table 4 Thermal properties of PETG

Thermal properties	Filament PETG
Thermal conductivity (k) [W/m.K]	0.2
Density (ρ) [Kg/m^3]	1250
Heat capacity (C_p) [$J/kg.K$]	1800

The material properties of C_p), ρ, and k are input for semi-transparent material properties. The thermal properties of the absorbent part are that of pure PETG, as seen in

Table 4. All the exposed surfaces are prescribed a convective heat flux boundary condition, with a heat transfer coefficient of h = 10[$W/(m^2.K)$.

The initial value for temperature is taken as the default room temperature, 23°C. Thermal insulation is applied on all the faces of the components except the interface. The heat source (Eq.(6), is determined by the beam laser distribution through 3D printed parts using the ray-tracing simulations. The intensity distribution data is applied as a function depending on the volume of the semi-transparent part and the area of the weld interface. This intensity is applied using a LiveLink™ for MATLAB® (see Fig. 9). That is the radiation source to simulate the temperature field in the COMSOL thanks to equation (5).

The displacement of the laser beam is considered parallel to the printing direction. In this case, that is perpendicular to the welding direction, the diffusion will affect strongly the temperature field.

Results and Discussion

Influence of void shape

This section uses the intensity distribution simulation at the interface obtained from the ray-tracing models. The ray tracing simulation (geometrical optic) are done with the mesh shown in Fig. 10. This mesh is used as RVE to carry out the paving of the overall sample geometry . Fig. 10 shows the intensity distribution of the laser beam before and after passing through the sample. The light scattering within the sample causes a redistribution of the laser intensity, leading to the formation of small slits where the laser intensity is significantly reduced. These slits are formed at locations where there are void grooves in the sample and are the results of the multiple refractions of the laser light at the air-matrix interfaces. In contrast, areas of the sample with no void grooves

Materials Research Proceedings 41 (2024) 2595-2606 https://doi.org/10.21741/9781644903131-285

allow the laser light to pass along straight paths with no scattering. In addition, these areas also receive intensities from the scattered zones, resulting in concentrated areas of laser light. Overall, the sample's microstructure influences the laser beam behavior and can result in complex intensity patterns that depend on the presence or absence of the void grooves. It can also be seen in Fig. 10a, b, and c that the ray-tracing model effectively simulates this feature.

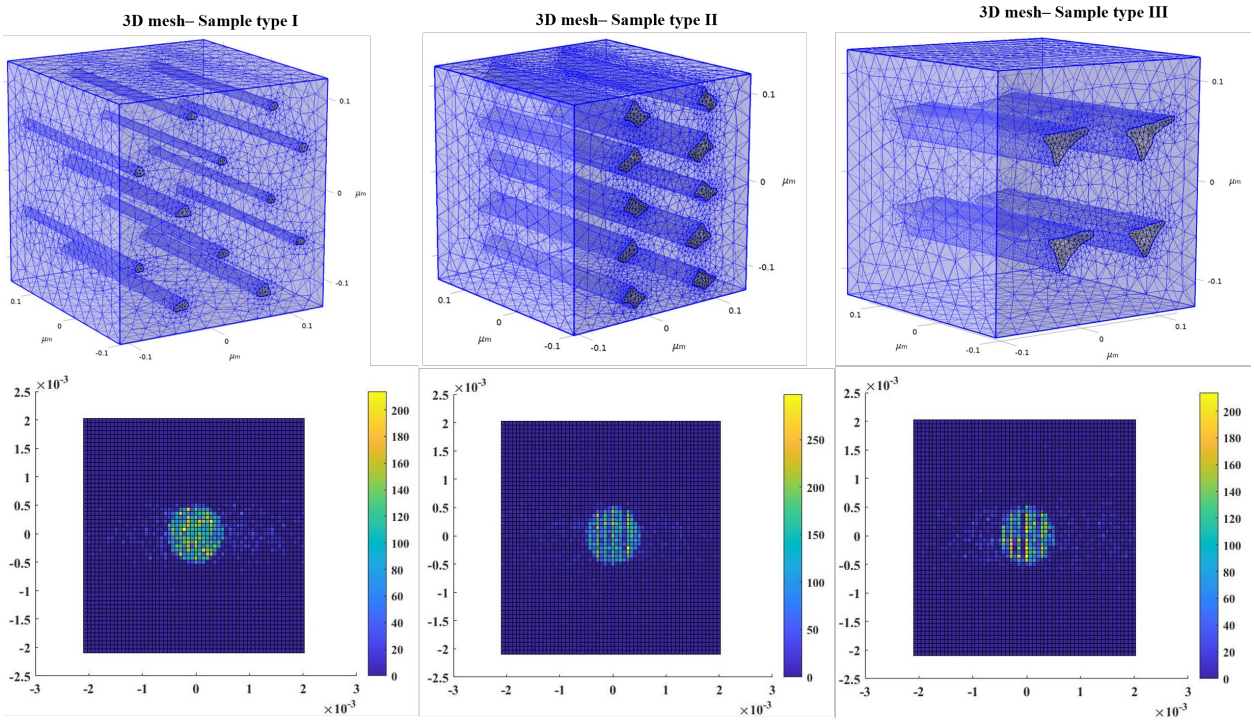

Fig. 10 Comparison of simulated laser intensity for three sample types

The influence of the void shape on the intensity distribution map of the laser beam at the weld interface is shown in Fig. 10. It is observed that the size of the slits, where the laser intensity is reduced, is a function of the voids' form. As a result, the ones observed that the laser beam distribution of the sample type I is more concentrated than samples II and III are for sample II. Accordingly, for the sample II, the light scattering in concentrated areas reaches higher peaks (Fig. 10).

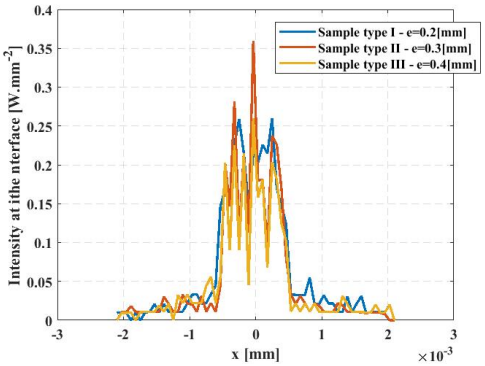

Fig. 11 The intensity distribution at the interface of three results

Influence of the scattering effect on the weld quality

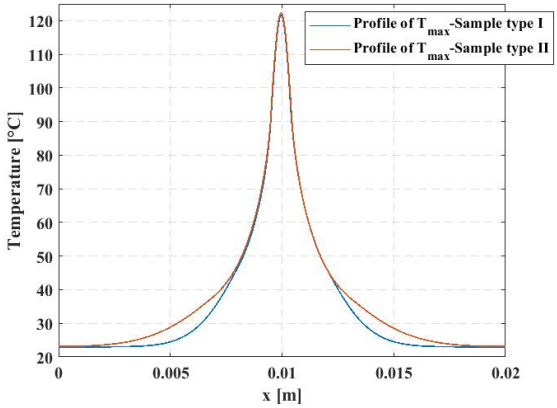

Fig. 12 Comparison of simulated maximum temperature profiles

For the sake of comparison, Fig. 12 shows the thermal simulations for two different types the sample types I and II with a thickness 2mm. Based on the results, observing the orange line, we can see that the energy distribution reaching the weld interface is more diffused compared to the blue line. It means that the quality of the weld seam is directly influenced by the porosity of the 3D printing process during the welding process. This confirms that the non-homogenization of the intensity distribution due to the scattering effect. Consequently, the weld quality along the seam line width is seriously impacted.

Conclusion

The structural layer-by-layer process of the 3D printing procedure results in a complex heterogeneous microstructure with a larger amount of porosity within the 3D printed parts. Consequently, laser intensity is subjected to scattering effects when propagating through the thickness of the 3D-printed components during the TLW process. Clearly, understanding the effects of light scattering allows for the control of the interface weld temperature to achieve high-quality assembly.

In this study, we have explored the influence of 3D printing process parameters on the microstructure, specifically the void shape, of 3D printed thermoplastic parts. Subsequently, we have investigated three types of void morphologies in 3D-oriented parts to examine the light-scattering effects of each sample type.

We have introduced a ray-tracing model capable of simulating light-scattering phenomena during the transmission of laser intensity through a semi-transparent sample. This proposed model can predict the laser beam reaching the interface during TLW, allowing for the consideration of differences in the microstructure among various sample types. The influence of void shape is also examined, demonstrating the growing impact of light-scattering effects with variable voids.

To assess the influence of the scattering effect on weld quality, 3D thermal simulations are conducted to predict the temperature field during the TLW process. Results indicate a noticeable reduction in weld quality due to the scattering effect.

Future work will involve using the ray-tracing model coupled with a FEM model to simulate the temperature field during the TLW process of 3D CCFRCs.

Acknowledgments

The authors extend their sincere appreciation to the National French Research Agency's ANR JCJC program for funding the SHORYUKEN project (Grant agreement n° ANR-21-CE10-0007-01) through AAPG 2021—CE10 “Industrie et Usine du Futur: Homme, Organisation, Technologies” initiative. Without their support, this work would not have been possible.

Reference:

[1] André Chateau Akué Asséko, Benoît Cosson, Éric Lafranche, Fabrice Schmidt, and Yannick Le Maoult. 2016. Effect of the developed temperature field on the molecular interdiffusion at the interface in infrared welding of polycarbonate composites. *Compos. Part B Eng.* 97, (July 2016), 53–61. https://doi.org/10.1016/j.compositesb.2016.04.064

[2] André Chateau Akué Asséko, Benoît Cosson, Fabrice Schmidt, Yannick Le Maoult, Rémi Gilblas, and Eric Lafranche. 2015. Laser transmission welding of composites – Part B: Experimental validation of numerical model. *Infrared Phys. Technol.* 73, (November 2015), 304–311. https://doi.org/10.1016/j.infrared.2015.10.005

[3] France Chabert, Christian Garnier, Jules Sangleboeuf, André Chateau Akue Asseko, and Benoît Cosson. 2020. Transmission Laser Welding of Polyamides: Effect of Process Parameter and Material Properties on the Weld Strength. *Procedia Manuf.* 47, (January 2020), 962–968. https://doi.org/10.1016/j.promfg.2020.04.297

[4] J. M. Chacón, M. A. Caminero, P. J. Núñez, E. García-Plaza, I. García-Moreno, and J. M. Reverte. 2019. Additive manufacturing of continuous fibre reinforced thermoplastic composites using fused deposition modelling: Effect of process parameters on mechanical properties. *Compos. Sci. Technol.* 181, (September 2019), 107688. https://doi.org/10.1016/j.compscitech.2019.107688

[5] Yu Chen, Oğuzhan Çopuroğlu, Claudia Romero Rodriguez, Fernando F. de Mendonca Filho, and Erik Schlangen. 2021. Characterization of air-void systems in 3D printed cementitious materials using optical image scanning and X-ray computed tomography. *Mater. Charact.* 173, (March 2021), 110948. https://doi.org/10.1016/j.matchar.2021.110948

[6] Yu Chen, Oğuzhan Çopuroğlu, Claudia Romero Rodriguez, Fernando F. de Mendonca Filho, and Erik Schlangen. 2021. Characterization of air-void systems in 3D printed cementitious materials using optical image scanning and X-ray computed tomography. *Mater. Charact.* 173, (March 2021), 110948. https://doi.org/10.1016/j.matchar.2021.110948

[7] Benoît Cosson, André Chateau Akué Asséko, Mylène Lagardère, and Myriam Dauphin. 2019. 3D modeling of thermoplastic composites laser welding process – A ray tracing method coupled with finite element method. *Opt. Laser Technol.* 119, (November 2019), 105585. https://doi.org/10.1016/j.optlastec.2019.105585

[8] Benoit Cosson, Mylène Deléglise, and Wolfgang Knapp. 2015. Numerical analysis of thermoplastic composites laser welding using ray tracing method. *Compos. Part B Eng.* 68, (January 2015), 85–91. https://doi.org/10.1016/j.compositesb.2014.08.028

[9] M. Ilie, E. Cicala, D. Grevey, S. Mattei, and V. Stoica. 2009. Diode laser welding of ABS: Experiments and process modeling. *Opt. Laser Technol.* 41, 5 (July 2009), 608–614. https://doi.org/10.1016/j.optlastec.2008.10.005

[10] Mariana Ilie, Jean-Christophe Kneip, Simone Matteï, Alexandru Nichici, Claude Roze, and Thierry Girasole. 2007. Laser beam scattering effects in non-absorbent inhomogenous polymers. *Opt. Lasers Eng.* 45, 3 (March 2007), 405–412. https://doi.org/10.1016/j.optlaseng.2006.07.004

[11] Julian Kuklik, Torben Mente, Verena Wippo, Peter Jaeschke, Benjamin Kuester, Malte Stonis, Stefan Kaierle, and Ludger Overmeyer. 2022. Laser welding of additively manufactured thermoplastic components assisted by a neural network-based expert system. In *High-Power Laser Materials Processing: Applications, Diagnostics, and Systems XI*, March 04, 2022. SPIE, 119–124. . https://doi.org/10.1117/12.2609365

[12] Anh-Duc Le, André Chateau Akué Asséko, Thi-Ha-Xuyen Nguyen, and Benoît Cosson. 2023. Laser intensity and surface distribution identification at weld interface during laser transmission welding of thermoplastic polymers: A combined numerical inverse method and

experimental temperature measurement approach. *Polym. Eng. Sci.* 63, 9 (2023), 2795–2805. https://doi.org/10.1002/pen.26405

[13] Anh-Duc Le, Benoît Cosson, and André Chateau Akué Asséko. 2021. Simulation of large-scale additive manufacturing process with a single-phase level set method: a process parameters study. *Int. J. Adv. Manuf. Technol.* 113, 11 (April 2021), 3343–3360. https://doi.org/10.1007/s00170-021-06703-5

[14] I. Maskery, N. T. Aboulkhair, M. R. Corfield, C. Tuck, A. T. Clare, R. K. Leach, R. D. Wildman, I. A. Ashcroft, and R. J. M. Hague. 2016. Quantification and characterisation of porosity in selectively laser melted Al–Si10–Mg using X-ray computed tomography. *Mater. Charact.* 111, (January 2016), 193–204. https://doi.org/10.1016/j.matchar.2015.12.001

[15] M. Parker, A. Inthavong, E. Law, S. Waddell, N. Ezeokeke, R. Matsuzaki, and D. Arola. 2022. 3D printing of continuous carbon fiber reinforced polyphenylene sulfide: Exploring printability and importance of fiber volume fraction. *Addit. Manuf.* 54, (June 2022), 102763. https://doi.org/10.1016/j.addma.2022.102763

[16] Mojtaba Salehi, Saeed Maleksaeedi, Mui Ling Sharon Nai, and Manoj Gupta. 2019. Towards additive manufacturing of magnesium alloys through integration of binderless 3D printing and rapid microwave sintering. *Addit. Manuf.* 29, (October 2019), 100790. https://doi.org/10.1016/j.addma.2019.100790

[17] John R. Howell Siegel M. Pinar Mengüc, Kyle Daun, Robert. 2020. *Thermal Radiation Heat Transfer* (7th ed.). CRC Press, Boca Raton. https://doi.org/10.1201/9780429327308

[18] Valérie Vancauwenberghe, Victor Baiye Mfortaw Mbong, Els Vanstreels, Pieter Verboven, Jeroen Lammertyn, and Bart Nicolai. 2019. 3D printing of plant tissue for innovative food manufacturing: Encapsulation of alive plant cells into pectin based bio-ink. *J. Food Eng.* 263, (December 2019), 454–464. https://doi.org/10.1016/j.jfoodeng.2017.12.003

[19] Zhenhu Wang, Yaohui Wang, Jian He, Ke Dong, Guoquan Zhang, Wenhao Li, and Yi Xiong. 2023. Additive Manufacturing of Continuous Fiber-Reinforced Polymer Composite Sandwich Structures with Multiscale Cellular Cores. *Chin. J. Mech. Eng. Addit. Manuf. Front.* 2, 3 (September 2023), 100088. https://doi.org/10.1016/j.cjmeam.2023.100088

[20] Nekoda van de Werken, Halil Tekinalp, Pouria Khanbolouki, Soydan Ozcan, Andrew Williams, and Mehran Tehrani. 2020. Additively manufactured carbon fiber-reinforced composites: State of the art and perspective. *Addit. Manuf.* 31, (January 2020), 100962. https://doi.org/10.1016/j.addma.2019.100962

[21] Siwon Yu, Yun Hyeong Hwang, Jun Yeon Hwang, and Soon Hyung Hong. 2019. Analytical study on the 3D-printed structure and mechanical properties of basalt fiber-reinforced PLA composites using X-ray microscopy. *Compos. Sci. Technol.* 175, (May 2019), 18–27. https://doi.org/10.1016/j.compscitech.2019.03.005

[22] Soudage laser par transmission de composites. *Techniques de l'Ingénieur*. Retrieved January 11, 2024 from https://www.techniques-ingenieur.fr/base-documentaire/materiaux-th11/plasturgie-procedes-specifiques-aux-composites-42474210/soudage-laser-par-transmission-de-composites-am5232/